Journal of Zhejiang University-SCIENCE B (Biomedicine & Biotechnology) *2021 22(10):818-838*
www.jzus.zju.edu.cn; www.springer.com/journal/11585
E-mail: jzus_b@zju.edu.cn

Research Article

https://doi.org/10.1631/jzus.B2100130

Check for updates

Low-intensity pulsed ultrasound ameliorates angiotensin II-induced cardiac fibrosis by alleviating inflammation via a caveolin-1-dependent pathway

Kun ZHAO[1], Jing ZHANG[1], Tianhua XU[1], Chuanxi YANG[1], Liqing WENG[1], Tingting WU[1], Xiaoguang WU[1], Jiaming MIAO[2], Xiasheng GUO[2], Juan TU[2], Dong ZHANG[2], Bin ZHOU[1,3]✉, Wei SUN[1]✉, Xiangqing KONG[1]

[1]*Department of Cardiology, the First Affiliated Hospital of Nanjing Medical University, Nanjing 210029, China*
[2]*Key Laboratory of Modern Acoustics, Department of Physics, Collaborative Innovation Center of Advanced Microstructure, Nanjing University, Nanjing 210093, China*
[3]*Departments of Genetics, Pediatrics, and Medicine (Cardiology), Wilf Cardiovascular Research Institute, Albert Einstein College of Medicine, Bronx, NY 10461, USA*

Abstract: Objective: Cardiac hypertrophy and fibrosis are major pathological manifestations observed in left ventricular remodeling induced by angiotensin II (AngII). Low-intensity pulsed ultrasound (LIPUS) has been reported to ameliorate cardiac dysfunction and myocardial fibrosis in myocardial infarction (MI) through mechano-transduction and its downstream pathways. In this study, we aimed to investigate whether LIPUS could exert a protective effect by ameliorating AngII-induced cardiac hypertrophy and fibrosis and if so, to further elucidate the underlying molecular mechanisms. Methods: We used AngII to mimic animal and cell culture models of cardiac hypertrophy and fibrosis. LIPUS irradiation was applied in vivo for 20 min every 2 d from one week before mini-pump implantation to four weeks after mini-pump implantation, and in vitro for 20 min on each of two occasions 6 h apart. Cardiac hypertrophy and fibrosis levels were then evaluated by echocardiographic, histopathological, and molecular biological methods. Results: Our results showed that LIPUS could ameliorate left ventricular remodeling in vivo and cardiac fibrosis in vitro by reducing AngII-induced release of inflammatory cytokines, but the protective effects on cardiac hypertrophy were limited in vitro. Given that LIPUS increased the expression of caveolin-1 in response to mechanical stimulation, we inhibited caveolin-1 activity with pyrazolopyrimidine 2 (pp2) in vivo and in vitro. LIPUS-induced downregulation of inflammation was reversed and the anti-fibrotic effects of LIPUS were absent. Conclusions: These results indicated that LIPUS could ameliorate AngII-induced cardiac fibrosis by alleviating inflammation via a caveolin-1-dependent pathway, providing new insights for the development of novel therapeutic apparatus in clinical practice.

Key words: Low-intensity pulsed ultrasound (LIPUS); Caveolin-1; Cardiac fibrosis; Inflammation; Angiotensin II (AngII)

1 Introduction

As an adaptive response of the heart to various physiological or pathological stimuli, cardiac remodeling can normalize increased wall stress of the left ventricle (LV), resulting in decompensated heart failure (Shimizu and Minamino, 2016; Nakamura and Sadoshima, 2018). This has been considered one of the most common causes of mortality worldwide. The progression of cardiac remodeling is characterized by cardiac hypertrophy and myocardial fibrosis, which are closely related to mechanical stress and neurohumoral stimulation (Saucerman et al., 2019).

Angiotensin II (AngII) is a vital octapeptide of the renin-angiotensin system (RAS), which facilitates cardiac remodeling in vivo and in vitro via key molecular mechanisms involved in the oxidative stress, cell apoptosis, and inflammatory responses (Schlüter and Wenzel, 2008; Ames et al., 2019).

The release and activation of transforming growth factor-β (TGF-β) and other transcription factors induced by AngII play crucial roles in promoting the deposition of extracellular matrix (ECM) in fibrosis, thereby

✉ Wei SUN, weisun7919@njmu.edu.cn
Bin ZHOU, bin.zhou@einstein.yu.edu
Wei SUN, https://orcid.org/0000-0003-0833-0445
Bin ZHOU, https://orcid.org/0000-0002-5486-2285

Received Feb. 4, 2021; Revision accepted July 1, 2021;
Crosschecked Aug. 30, 2021

mediating cardiac structural remodeling in an auto/paracrine manner (Rosenkranz, 2004; Sweeney et al., 2020).

Although there have been many therapeutic methods targeting the pathogenetic mechanism of pathological cardiac remodeling in the clinic, adequate and effective treatment modalities for this disease are still lacking (Zhao et al., 2020). Therefore, the discovery of novel therapeutic targets would be valuable.

In addition to the diagnostic role of ultrasound, low-intensity pulsed ultrasound (LIPUS), a safe and noninvasive method of mechanical stimulation, has been studied and widely applied to treat various diseases clinically through regulating inflammatory responses and downstream intracellular signaling pathways (Xu et al., 2019; Zheng et al., 2019; Monma et al., 2021). Studies have revealed that LIPUS therapy can attenuate and reverse cardiac dysfunction, and ameliorate myocardial fibrosis in animal models of myocardial infarction (MI) and transverse aortic constriction (TAC) through the involvement of mechano-transduction and activation of the p38 mitogen-activated protein kinase (MAPK) signaling pathways (Shindo et al., 2016; Ogata et al., 2017). Moreover, repetitive LIPUS irradiation has a positive therapeutic effect not only on chronic myocardial ischemia, but also on nonischemic heart diseases, such as hypertensive heart disease, through therapeutic angiogenesis and/or mediation of caveolin-1 (Jiang et al., 2019). Considering the complex and different pathogenesis contributing to myocardial fibrosis (Ma et al., 2018), it was unclear whether LIPUS could attenuate AngII-induced cardiac fibrosis as well.

As an important functional protein on the cell membrane for sensing mechanical stimuli, including cell stretch induced by LIPUS irradiation, caveolin-1 is the main component of caveolae involved in the mechano-transduction process (Grivas et al., 2020). Caveolin-1 is directly responsible for the physiological and pathological function of human fibroblasts through mediating the activation of various key signaling molecules and signaling pathways, such as nitric oxide synthase (NOS) and G-protein subunits (Shi et al., 2016; Ding et al., 2017; Forrester et al., 2017). In addition to responding to mechanical stress by interacting with β1-integrin, recent studies have also reported that caveolin-1 can regulate inflammatory responses that contribute to fibrotic diseases via MAPK signaling (Jokhadar et al., 2013; Wang et al., 2016; Chinnakkannu et al., 2018). However, it was unknown whether LIPUS irradiation could improve AngII-induced cardiac remodeling through caveolin-1-mediated mechano-transduction and its downstream pathways.

Thus, in our study, we investigated the role of LIPUS in AngII-induced cardiac remodeling and explored its mechanisms.

2 Materials and methods

2.1 Animal care

After being approved by the Experimental Animals Use and Care Committee of Nanjing Medical University (Nanjing, China), the 4–6-week-old wild-type (WT) C57BL/6J male mice (Vital River Biological Co., Ltd., Beijing, China) were used for in vivo experiments following the recommendations listed in the National Institutes of Health Guide for the Care and Use of Laboratory Animals. All the animals were housed in a reverse light-dark cycle (12 h per stage) with food and water available ad libitum.

2.2 Study design and grouping

The mice were randomly divided into different groups according to their weights. They were then implanted with an ALZET 2004 osmotic mini-pump (Durect Corp., Cupertino, CA, USA), filled with either AngII (2.5 mg/(kg·d)) or phosphate-buffered saline (PBS), subcutaneously under inhalation anesthesia with isoflurane, and the contents were delivered at the rate of 0.25 μL/h for four successive weeks. PBS was administered in the control group, and the infusion rate of AngII was determined according to the description by Chinnakkannu et al. (2018). The treatment group and the LIPUS control group underwent LIPUS irradiation (described below) for 20 min under isoflurane anesthesia every 2 d from one week before mini-pump implantation to four weeks after mini-pump implantation (Zhao et al., 2021). The sham group and model group underwent the same anesthesia, but without LIPUS irradiation. After evaluating cardiac function by echocardiography at the end of four weeks, the heart samples were collected from the mice euthanized by CO_2 inhalation. Thereafter, the atrium was removed, and the LV isolated. Frozen tissue samples were used for western blotting (WB) and quantitative real-time polymerase chain reaction (qPCR) analyses, while

formalin-fixed and paraffin-embedded tissue samples were used for Sirius Red staining, hematoxylin and eosin (H&E) staining, Masson's staining, and immunofluorescence staining.

2.3 Cell isolation and culture

Fresh neonatal rat cardiomyocytes (NRCMs) and neonatal rat cardiac fibroblasts (NRCFs) were isolated from 1- to 3-d-old newborn Sprague-Dawley (SD) rats (Vital River Biological Co., Beijing, China) as previously described (Vandergriff et al., 2015; Wang et al., 2017). Then, about 4×10^5 NRCMs were seeded and cultured in 60-mm cell culture dishes with Dulbecco's modified Eagle's medium (DMEM; Gibco Co., USA) containing 10% (volume fraction) horse serum (HS; Gibco Co.), 5% (volume fraction) fetal bovine serum (FBS; HyClone Co., USA), and 1% (volume fraction) penicillin-streptomycin (P/S; HyClone Co.).

On the second day of culture, NRCMs were incubated in serum-free DMEM with overnight starvation before further experiments. Then, the treatment group and LIPUS control group were exposed to LIPUS irradiation for 20 min on each of two occasions 6 h apart. After that, the model group and treatment group underwent induction with L mmol/L of AngII (Sigma-Aldrich Co., USA) for 48 h.

In some experiments, cells were pre-incubated with 10 μmol/L of pyrazolopyrimidine 2 (pp2; S7008, Selleck Co., China) and/or 1 μmol/L TLR4 inhibitor TAK-242 (soluble in dimethyl sulfoxide (DMSO), Selleck Co.) for 2–3 h or 1 ng/mL reconstituted lyophilized recombinant rat interleukin-1β (rRtIL-1β)/rRtIL-6 for 12 h prior to LIPUS irradiation. Caveolin-1 small interfering RNA (siRNA) (si-caveolin-1) and control siRNA, purchased from RiboBio Co. (Guangzhou, China), were used in other experiments. When the cells reached 60%–70% confluence, 50 nmol/L si-caveolin-1 was transfected into cells for 6–8 h with Lipofectamine® RNAiMAX (Invitrogen, Carlsbad, CA, USA) following the instructions provided.

NRCFs were also seeded in 60-mm cell culture dishes, but cultured in fibroblast medium (FM; Sciencell Co., China). They were treated identically to NRCMs in subsequent experiments.

The cell samples were collected for WB, qPCR, enzyme-linked immunosorbent assay (ELISA), and immunofluorescence analyses.

2.4 Echocardiography

The left ventricular function, including left ventricular fractional shortening (LVFS), left ventricular ejection fraction (LVEF), left ventricular internal diameters at end systole (LVIDs), left ventricular internal diameters at end diastole (LVIDd), left ventricular end-systolic volume (LVESV), cardiac output (CO), and mitral annular plane systolic excursion (MAPSE) measurement, was evaluated in the mice receiving different treatments by calculating the transthoracic echocardiographic images obtained using the Vevo 3100 ultrasound and photoacoustic imaging system (VisualSonics, Toronto, Canada).

2.5 Western blotting

The bicinchoninic acid (BCA) method (Pierce Biotechnology, Inc., Rockford, IL, USA) was used to assay the protein concentration of the supernatant collected from the homogenized isolated tissues or cells.

Equal amounts of proteins (30 μg) mixed with loading buffer were separated by electrophoresis using 10% (0.1 g/mL) sodium dodecyl sulfate-polyacrylamide gel electrophoresis (SDS-PAGE) and then transferred to polyvinylidene fluoride (PVDF) membranes. After blocking with 5% (volume fraction) defatted milk for 2 h at room temperature, the membranes were incubated overnight at 4 °C with primary antibodies (1:1000 dilution, volume ratio, the same below) against α-smooth muscle actin (α-SMA; Cell Signaling Technology, USA), collagen I (Beyotime Biotechnology, Shanghai, China), TGF-β (Beyotime Biotechnology), vascular endothelial growth factor (VEGF; Cell Signaling Technology), caveolin-1 (Cell Signaling Technology), interleukin-6 (IL-6; Proteintech Co., Wuhan, China), IL-1β (Proteintech Co.), tumor necrosis factor-α (TNF-α; Proteintech Co.), phospho-caveolin-1 (Tyr14; Cell Signaling Technology), or glyceraldehyde-3-phosphate dehydrogenase (GAPDH; Beyotime Biotechnology). Following incubation with horseradish peroxidase (HRP)-conjugated secondary antibodies (1:5000 dilution) for 2 h at room temperature and washing in Tris-buffered saline, the blots were detected with enhanced chemiluminescence reagent (ThermoFisher Co., USA) with an optimal exposure time. The intensity of protein bands was analyzed and normalized to that of GAPDH using ImageJ software.

2.6 qPCR analysis

The TRIzol (Invitrogen Life Technologies, Carlsbad, CA, USA) was used to extract total RNA from the cells or heart samples in accordance with the manufacturer's instructions. A total of 0.5 mg of RNA was reverse-transcribed into complementary DNAs (cDNAs). Then, qPCR was performed using an Applied Biosystems 7900HT fast real-time PCR system (Carlsbad, CA, USA). The $2^{-\Delta\Delta C_T}$ method was adopted to quantify the messenger RNA (mRNA) levels of each gene. The primers are listed in Table S1.

2.7 Low-intensity pulsed ultrasound stimulation

LIPUS irradiation was performed using an ultrasound machine including an ultrasonic generator (Agilent Technologies, Santa Clara, CA, USA), a broadband power amplifier (Verasonics, Inc., USA), and a planar transducer (Haifu, Chongqing, China). LIPUS stimulation was applied for 20 min at a planar transducer frequency of 0.5 MHz and an intensity of 19.30–120.63 mW/cm^2 in 10-ms pulse bursts (Table S2). The number of cycles was 100, and the spatial-temporal average sound pressure was 0.3 MPa. The 60-mm culture dishes seeded with cells were placed on the top of the transducer filled with deaerated water. A temperature test paper (TMCHallcrest, USA) was used to test the temperature of the culture media in the dishes. The results showed that there were hardly any changes in temperature under our ultrasound conditions during the LIPUS procedures (Figs. S1 and S2).

2.8 Flow cytometry

After the different treatments, all the viable cells and cell debris were collected and then stained with propidium iodide (PI) and Annexin-V (Fcmacs Biotech Co., China) in the dark for 25 min in accordance with the provided instructions. After that, we used the flow cytometry to semi-quantify the degree of cell apoptosis.

2.9 Masson staining and Sirius Red staining

After dewaxing and rehydration, formalin-fixed and paraffin-embedded tissue sections (5-μm thick) were stained with Masson staining and Sirius Red staining (Service Biological Technology Co., Ltd., Wuhan, China) using standard procedures. Then, to assess the percentage of myocardial fibrosis, images of more than three randomly selected whole-sections were taken with a Zeiss fluorescence upright microscope (Carl Zeiss, Jena, Germany) and measured with Image-Pro Plus software (Version 6.0; Media Cybernetics, Inc., Bethesda, MD, USA).

2.10 Wheat germ agglutinin and H&E staining

To determine the area of cardiomyocyte cross-sections, deparaffinized and rehydrated paraffin-embedded sections were stained with wheat germ agglutinin (WGA) Alexa Fluor 647 (1∶500 dilution; Invitrogen Life Technologies) in combination with the secondary antibody and examined by H&E staining (Service Biological Technology Co., Ltd.) according to standard procedures. At least, five random fields were observed using a Zeiss fluorescence upright microscope (Carl Zeiss) and further analyzed using ImageJ software in a blinded manner.

2.11 Immunofluorescence analyses

NRCMs seeded in culture dishes were blocked with PBS containing 5% (volume fraction) goat serum, 5% (0.05 g/mL) bovine serum albumin (BSA), and 0.5% (volume fraction) Triton for 1 h at room temperature after fixation with 4% (4 g/mL) paraformaldehyde and permeabilization with 1% (volume fraction) Triton. Then, cells were incubated with anti-actinin antibody (1:150; Sigma-Aldrich Co., USA) and caveolin-1 (Cell Signaling Technology) overnight at 4 ℃, followed by incubation with rabbit immunoglobulin G (IgG) antibody (Alexa Fluor 488) and dilution with 4',6-diamidino-2-phenylindole (DAPI) at room temperature. After that, a Zeiss fluorescence inverted microscope was used to digitize more than three fields of view chosen at random within each group. The images were blindly analyzed with ImageJ software.

2.12 Superoxide dismutase, lactate dehydrogenase, and malondialdehyde activity assays

After centrifugation at 12 000*g* for 15 min, the supernatant liquid of the cell suspension was collected. Then, we used available ELISA kits (Service Biological Technology Co., Ltd.) to evaluate superoxide dismutase (SOD), lactate dehydrogenase (LDH), and malondialdehyde (MDA) concentrations according to the manufacturers' instructions.

2.13 Statistics analysis

Data are expressed as the mean±standard error of the mean (SEM). Statistical analyses were performed using GraphPad Prism 7.0 software (GraphPad software Inc., CA, USA). One-way analysis of variance (ANOVA) was applied to determine statistical significance for experiments with more than two groups, followed by Bonferroni's post-hoc test. *P*-value of <0.05 was considered statistically significant.

3 Results

3.1 Effect of LIPUS irradiation on AngII-induced cardiac fibrosis in vitro

To determine whether LIPUS irradiation has effects on AngII-induced cardiac hypertrophy or fibrosis in vitro, experiments were performed using rat cardiomyocytes and cardiac fibroblasts. First, flow cytometry was applied to detect the impact of different doses of ultrasound intensities on the apoptosis of cardiomyocytes and cardiac fibroblasts. The results showed that 120.63 mW/cm^2 LIPUS can promote apoptosis of both types of cells (Fig. 1a and Fig. S3). Therefore, the ultrasound intensity used in further studies was no more than 77.20 mW/cm^2. Then, increased protein expression and mRNA levels of TGF-β and collagen I in cardiac fibroblasts induced by AngII were downregulated by LIPUS irradiation dose dependently (Figs. 1b–1e). Furthermore, following the treatment with/without LIPUS and/or AngII, immunostaining of cardiomyocytes with α-actinin showed that LIPUS irradiation did not significantly inhibit AngII-induced hypertrophic growth of cardiomyocytes (Fig. 1f). Next, qPCR results showed that LIPUS irradiation inhibited mRNA levels of atrial natriuretic peptide (ANP) and B-type natriuretic peptide (BNP) in cardiomyocytes following AngII induction dose dependently (Figs. 1g and 1h). However, the increased mRNA levels of β-myosin heavy chain (β-MHC) and α-MHC were not significantly ameliorated by LIPUS irradiation (Figs. 1i and 1j). These findings demonstrate that while LIPUS could play a protective role in AngII-induced cardiac fibrosis, it had a limited effect on cardiac hypertrophy in vitro. Subsequently, considering all the data shown above, cardiac fibroblasts were chosen as the main experimental subjects, and 77.20 mW/cm^2 was selected as the most appropriate ultrasonic intensity for the following experiments in vivo and in vitro.

3.2 Effect of LIPUS irradiation on AngII-induced cardiac hypertrophy in mice in vivo

We used an AngII-infused mouse model to investigate whether established cardiac remodeling induced by chronic AngII infusion in vivo could be inhibited by LIPUS irradiation (Fig. 2a). First, following AngII infusion for four weeks, the significant continuous weight loss observed in mice in the model group was reduced by LIPUS irradiation to a certain degree (Fig. 2b). The echocardiographic data also showed that LIPUS irradiation ameliorated AngII-induced cardiac dysfunction (Fig. 2c and Table 1). Moreover, the model group had adverse cardiac structural remodeling including grossly enlarged hearts (Fig. 2d) and increased ratios of heart weight (HW)/body weight (BW) and HW/tibia length (TL) compared with the control group, and LIPUS irradiation reduced these pathological indexes (Figs. 2e and 2f). A similar trend was seen in the mRNA expression of cardiac fetal genes, including *ANP*, *BNP*, *α-MHC*, and *β-MHC*, indicating a protective role of LIPUS irradiation in AngII-stimulated cardiac hypertrophy (Figs. 2g–2j). Furthermore, we measured the cross-sectional area of cardiomyocytes to determine the effect of LIPUS on myocyte hypertrophy by WGA and H&E staining. The quantitative analysis showed that LIPUS irradiation reduced the expanded myocyte cross-sectional area significantly following AngII infusion (Figs. 3a–3c).

3.3 Effect of LIPUS irradiation on AngII-induced myocardial fibrosis in mice in vivo

Fibrosis is known to result in phenotypic changes associated with pathological myocardial remodeling (Frangogiannis, 2021). Therefore, we examined the effect of LIPUS irradiation on AngII-induced myocardial and coronary artery fibroses in formalin-fixed and paraffin-embedded sections using Masson's staining method and Sirius Red staining. Analysis of the total collagen content showed that marked collagen deposition in LV tissues and coronary arteries could be visualized in the model group compared with the control group, while mice in the treatment group showed less collagen accumulation than those in the model group (Figs. 3d–3f and S4a). Furthermore, the protein expression of TGF-β and collagen I was assessed by

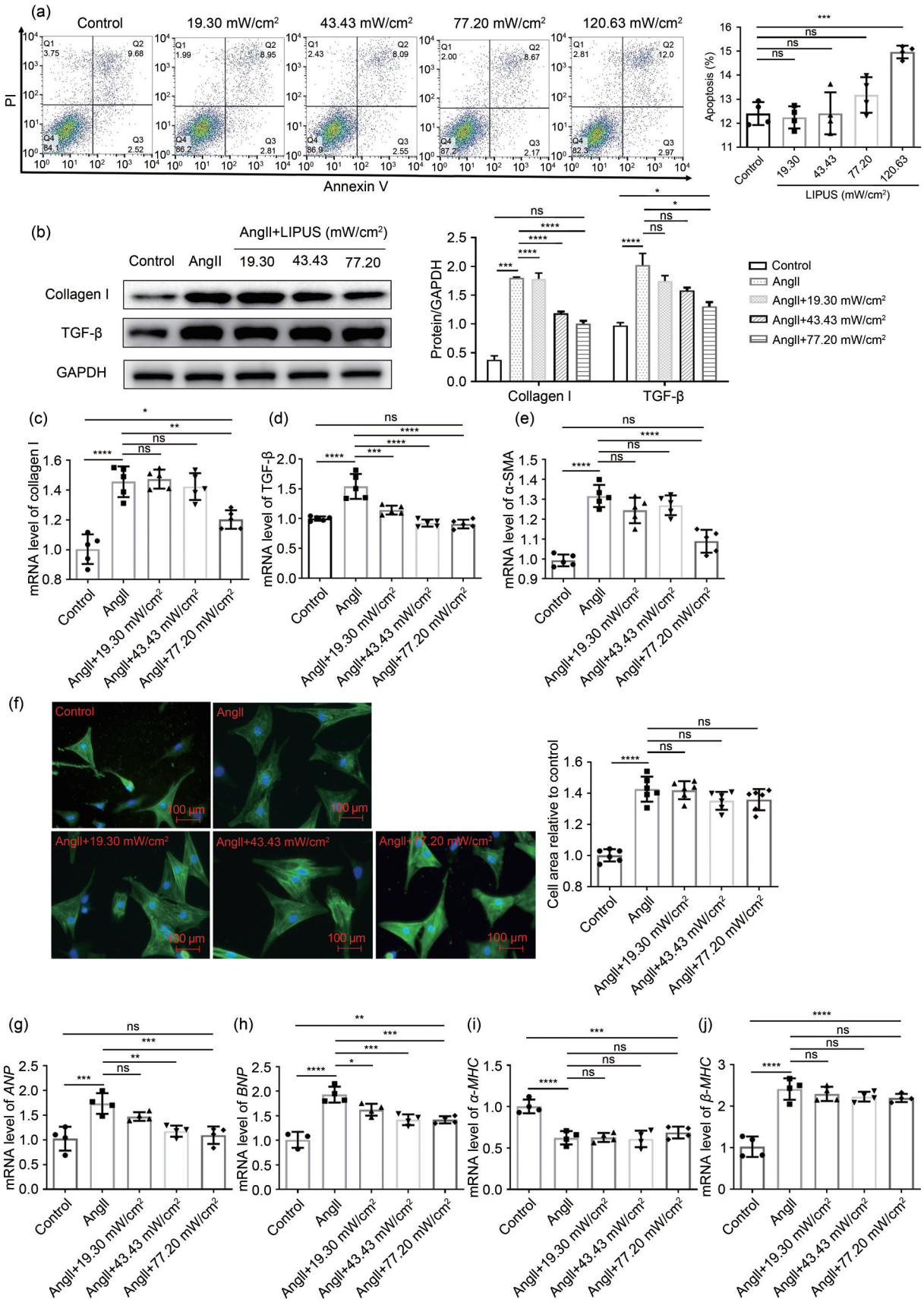
(a)
Control
19.30 mW/cm²
43.43 mW/cm²
77.20 mW/cm²
120.63 mW/cm²
PI
Annexin V
Apoptosis (%)
LIPUS (mW/cm²)
(b)
AngII+LIPUS (mW/cm²)
Control
AngII
19.30
43.43
77.20
Collagen I
TGF-β
GAPDH
Protein/GAPDH
Control
AngII
AngII+19.30 mW/cm²
AngII+43.43 mW/cm²
AngII+77.20 mW/cm²
(c)
mRNA level of collagen I
(d)
mRNA level of TGF-β
(e)
mRNA level of α-SMA
(f)
100 μm
Cell area relative to control
(g)
mRNA level of ANP
(h)
mRNA level of BNP
(i)
mRNA level of α-MHC
(j)
mRNA level of β-MHC

Fig. 1 Effects of LIPUS on ameliorating AngII-stimulated cardiac fibrosis and cardiac hypertrophy in vitro. (a) The flow cytometry showed the impact of different doses of ultrasound intensities on the apoptosis of NRCFs. (b) Protein levels of TGF-β and collagen I as determined by western blotting (left) in NRCFs from indicated groups and the corresponding densitometric analysis. (c–e) mRNA levels of collagen I (c), TGF-β (d), and α-SMA (e) in NRCFs from indicated groups determined by the qPCR method. (f) The cardiomyocytes labeled with α-actinin at 400× magnification (α-actinin, green; DAPI, blue) and their quantitative analyses. (g–j) mRNA levels of fetal genes *ANP* (g), *BNP* (h), *α-MHC* (i), and *β-MHC* (j) in cardiomyocytes from different groups. Results are presented as mean±standard error of the mean (SEM), $n>3$ per group. ns indicates being not significant; $^{*}P<0.05$, $^{**}P<0.01$, $^{***}P<0.001$, $^{****}P<0.0001$, compared with the control or model group. LIPUS, low-intensity pulsed ultrasound; AngII, angiotensin II; NRCF, neonatal rat cardiac fibroblast; α-SMA, α-smooth muscle actin; TGF-β, transforming growth factor β; qPCR, quantitative real-time polymerase chain reaction; DAPI, 4',6-diamidino-2-phenylindole; *ANP*, atrial natriuretic peptide; *BNP*, B-type natriuretic peptide; *MHC*, myosin heavy chain.

WB after normalization to GAPDH. We found that LIPUS irradiation reduced the increase in TGF-β and collagen I expression following AngII administration (Fig. 3g).

In addition, no obvious differences were found in cardiac structure or function between the LIPUS control group and the control group. These data suggested that LIPUS irradiation could attenuate and even revert cardiac hypertrophy and myocardial fibrosis in vivo.

3.4 Effect of LIPUS irradiation on AngII-induced cardiac fibrosis via caveolin-1

As caveolin-1 has been reported to be involved in mediating the beneficial effects of LIPUS in ameliorating postmyocardial infarction LV remodeling (Shindo et al., 2016), we next examined the contribution of caveolin-1 to the anti-remodeling effects of LIPUS. First, immunofluorescence showed that LIPUS, but not AngII treatment, increased the activation of caveolin-1 in cardiac fibroblasts in vivo and in vitro (Figs. 4a, 4b, 5a, and 5b). However, no obvious difference in caveolin-1 activation was found in cardiomyocytes among groups (Figs. 4c, 4d, 5c, and 5d). With regard to the frozen mice heart tissues, higher expression levels of VEGF and activated caveolin-1 were also found following LIPUS irradiation when compared with the control group (Figs. 4e and 4f). LIPUS irradiation also promoted the tyrosine-14 residue phosphorylation of caveolin-1, and increased total protein and mRNA expression of caveolin-1 in cardiac fibroblasts (Figs. 5e and 5f). However, no differences in caveolin-1 expression were observed between the control group and the model group. Subsequently, we used pp2 to suppress the expression of caveolin-1 to further investigate its contribution to the beneficial effect of LIPUS on cardiac fibrosis in NRCFs under AngII stimulation. Following pretreatment with pp2 or si-caveolin-1, the antifibrotic effects of LIPUS in cardiac fibroblasts were blocked in vitro (Figs. 5g, 5h, S5a, and S5b). In addition, pp2 or si-caveolin-1 pretreatment did not significantly interfere with the pathological effect of AngII in our study.

Then, LIPUS was applied on AngII-infused mice receiving pp2 (1.5 mg/kg intraperitoneal (i.p.)) (Lennmyr et al., 2004) or vehicle 30 min before each irradiation. The echocardiographic data showed that pp2 pretreatment inhibited the positive effects of LIPUS on ameliorating AngII-induced cardiac dysfunction (Fig. 6a and Table 2). A similar trend was seen in the mRNA expression of cardiac fetal genes (Fig. 6b). Then, WGA, Masson's method, and Sirius Red staining showed that pp2 pretreatment blocked the therapeutic effects of LIPUS on AngII-stimulated cardiac hypertrophy and fibrosis (Figs. 6c–6g). The WB verified the same observation (Fig. 6h). Also, pp2 pretreatment reversed the positive effects of LIPUS on AngII-induced coronary arteries to a certain extent (Fig. S4b). However, there were still significant differences between the AngII group and the AngII+LIPUS+pp2 group.

3.5 Effect of LIPUS irradiation on AngII-induced cardiac fibrosis by alleviating inflammation via a caveolin-1-dependent pathway

Since the inflammatory response has been shown to be vital in the progression of cardiac remodeling (Hanna and Frangogiannis, 2020), we next investigated the mRNA expression of several proinflammatory cytokines, including TNF-α, IL-1β, and IL-6, in cardiac fibroblasts by qPCR. Compared with the control group, there was a modest increase in the mRNA expression levels of TNF-α, IL-1β, and IL-6 following AngII administration, which was mitigated by pretreatment with LIPUS (Fig. 7a). We also tested the mRNA expression levels of proinflammatory cytokines in frozen mice heart samples. AngII-induced IL-1β and IL-6 expression, but not TNF-α expression, decreased with LIPUS irradiation (Fig. 7b). However, not all of

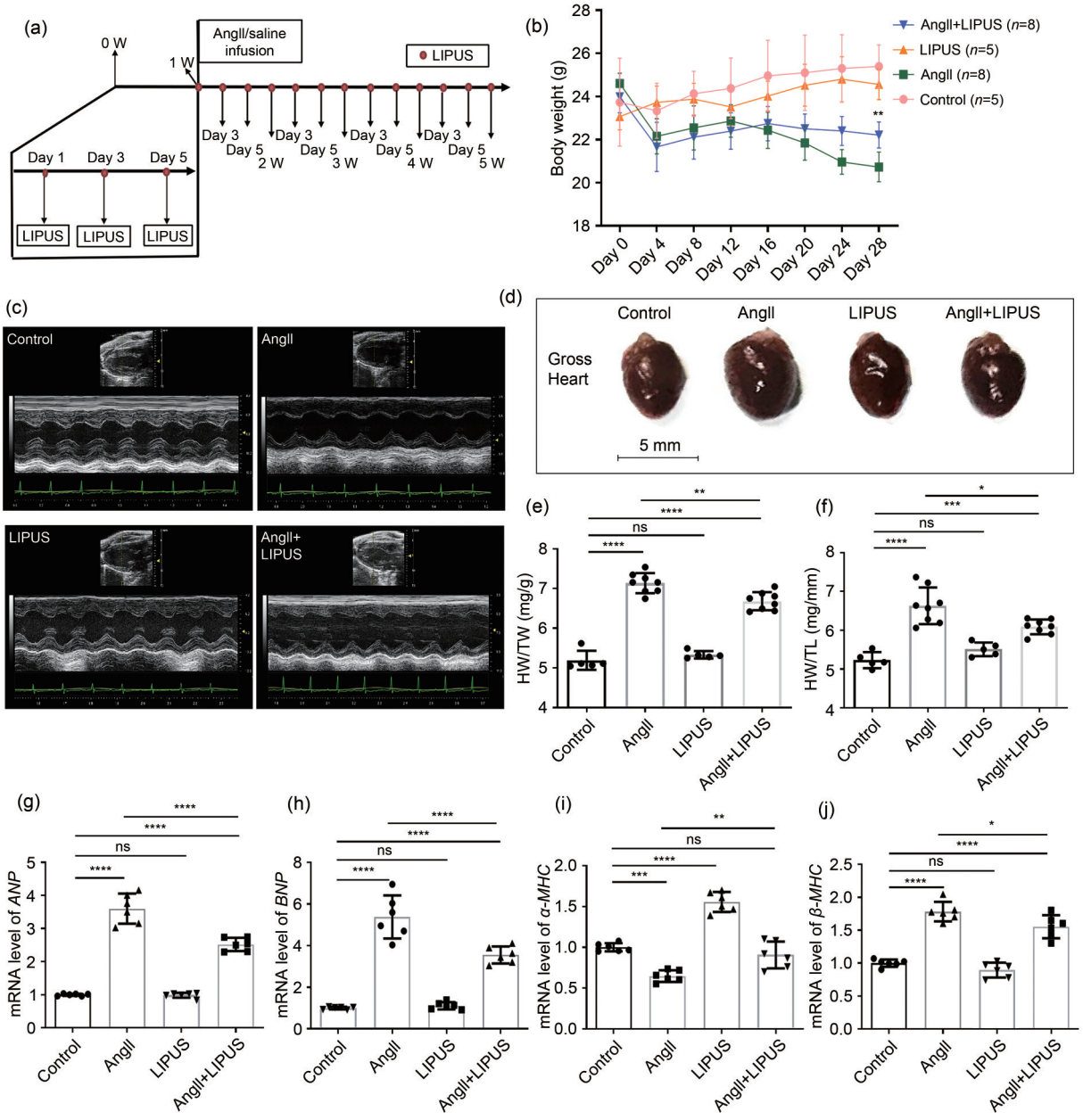

Fig. 2 Effects of LIPUS on ameliorating AngII-simulated cardiac hypertrophy in mice in vivo. (a) Study protocol. (b) Effect of LIPUS irradiation on body weight in AngII-induced mice. ** *P*<0.01 vs. AngII group. (c, d) Representative M-mode echocardiography images (c) and photographs (d) of the hearts from the control group (*n*=5), the LIPUS control group (*n*=8), the model group (*n*=8), and the treatment group (*n*=5). (e, f) Cardiac structure was assessed. (g–j) mRNA levels of fetal genes *ANP* (g), *BNP* (h), *α-MHC* (i), and *β-MHC* (j) in isolated mice hearts from indicated groups. Results are presented as mean±standard error of the mean (SEM), *n*>3 per group. ns indicates being not significant; ** *P*<0.01, * *P*<0.001, **** *P*<0.0001, compared with the control or model group. LIPUS, low-intensity pulsed ultrasound; AngII, angiotensin II; HW, heart weight; TW, total body weight; TL, tibia length; *ANP*, atrial natriuretic peptide; *BNP*, B-type natriuretic peptide; *MHC*, myosin heavy chain.**

these indexes reached the level of the control group. Then, we found that administration of TLR4 inhibitor TAK-242, which can decrease the mRNA levels of proinflammatory cytokines, could totally mimic the role of LIPUS irradiation in AngII-induced cardiac fibrosis (Figs. 7c and 7d), suggesting that LIPUS irradiation alleviated cardiac fibrosis by alleviating inflammation under AngII stimulation.

To verify the relationship between caveolin-1 and inflammation in the anti-fibrotic effects of LIPUS

Table 1 Echocardiographic data of left ventricular function four weeks after AngII infusion

Group	LVEF (%)	LVFS (%)	LVIDd (mm)	LVIDs (mm)	LVESV (mm)	MAPSE (mm)
Control	74.720±1.102	42.410±0.980	3.244±0.199	1.868±0.122	11.030±1.763	0.651±0.035
AngII	49.730±1.635*	24.790±0.964*	3.820±0.053*	2.876±0.072*	31.780±1.996*	0.474±0.020*
LIPUS	73.290±1.297	41.120±1.141	3.116±0.045	1.832±0.027	10.200±0.370	0.653±0.029
AngII+LIPUS	64.480±1.666#	33.980±1.224#	2.959±0.043#	1.952±0.019#	11.970±0.290#	0.615±0.029#

The results are presented as mean±standard error of the mean (SEM), n>3 per group. * P<0.05 vs. the control group; # P<0.05 vs. the model group. AngII, angiotensin II; LIPUS, low-intensity pulsed ultrasound; LVEF, left ventricular ejection fraction; LVFS, left ventricular fractional shortening; LVIDd, left ventricular internal diameters at end diastole; LVIDs, left ventricular internal diameters at end systole; LVESV, left ventricle end-systolic volume; MAPSE, mitral annular plane systolic excursion.

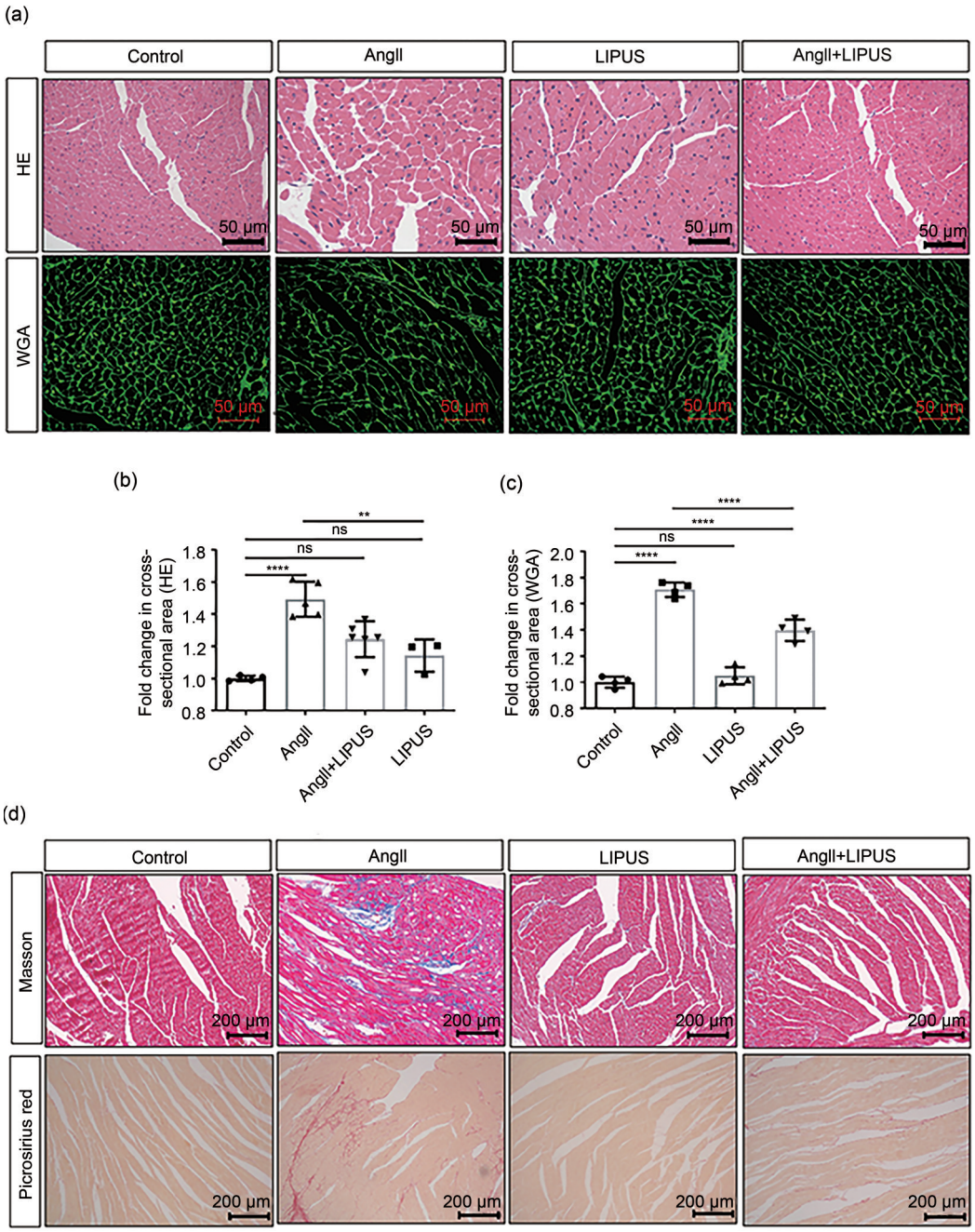

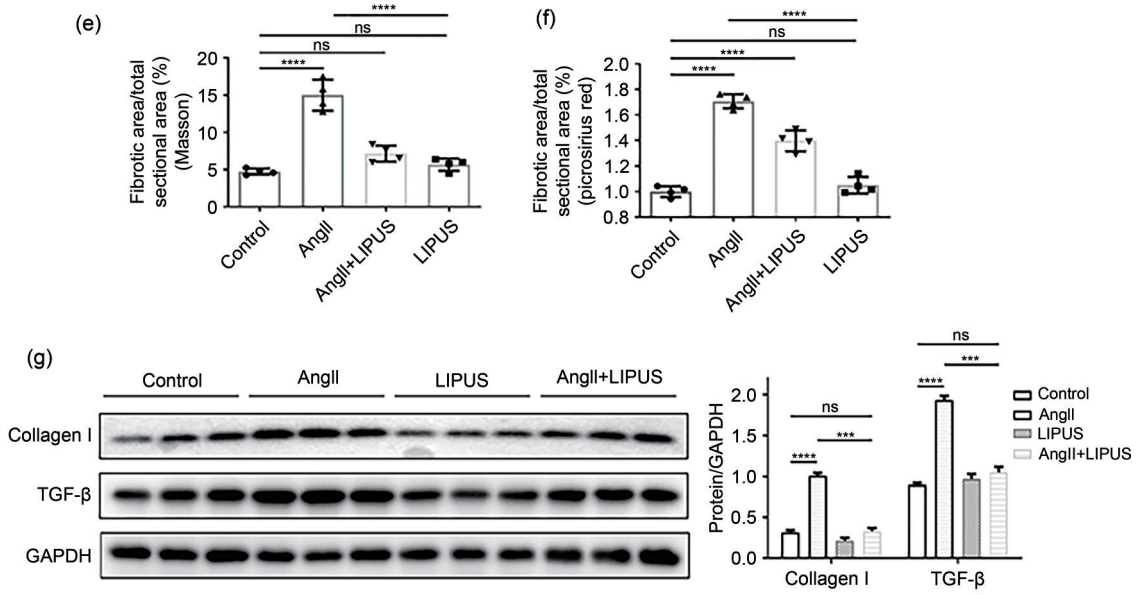

Fig. 3 Effects of LIPUS irradiation on ameliorating AngII-stimulated myocardial fibrosis in mice. (a) The longitudinal sections of LV tissue stained with hematoxylin and eosin (H&E) and wheat germ agglutinin (WGA) from indicated groups. (b, c) Quantitative analyses of the cardiomyocyte cross-sectional areas stained with H&E (b) and WGA (c). At least 50 cardiomyocytes per group (n>3 per group) were measured randomly using Image-Pro Plus software. (d) The longitudinal sections of LV tissue stained with Masson's method and picrosirius red from indicated groups. (e, f) Quantitative analyses of collagen deposition stained with Masson's method (e) and picrosirius red (f). (g) Protein levels of TGF-β and collagen I in the frozen mice hearts from different groups (n=6 per group) and their densitometric analyses. GAPDH was detected as the loading control. Results are presented as mean±standard error of the mean (SEM), n>3 per group. ns indicates being not significant; ** P<0.01, *** P<0.001, **** P<0.0001. LIPUS, low-intensity pulsed ultrasound; AngII, angiotensin II; LV, left ventricle; TGF-β, transforming growth factor-β; GAPDH, glyceraldehyde-3-phosphate dehydrogenase.

irradiation, we next used rRtIL-1β or rRtIL-6 to increase the expression of proinflammatory cytokines. The results showed that overexpression of IL-1β or IL-6 reversed the antifibrotic effects of LIPUS irradiation in vitro, but had insignificant effects on the expression of caveolin-1 (Figs. 7e and 7f). Furthermore, in vivo, we found that pp2 pretreatment could blunt the therapeutic effect of LIPUS irradiation on downregulating AngII-stimulated proinflammatory cytokine expression. Furthermore, in vivo, we found that pp2 pretreatment could blunt the thera-peutic effect of LIPUS irradiation on downregulating AngII-stimulated proinflammatory cytokine expression (Figs. 6i and 6j). Also, LIPUS-induced downregulation of the expression of proinflammatory cytokines in cardiac fibroblasts was blunted by pp2 or si-caveolin-1 pretreatment (Figs. 7g, 7h, and S5c). Taken collectively, these data suggested that LIPUS irradiation could exert its role in improving AngII-induced cardiac fibrosis via a caveolin-1-dependent pathway in vitro (Fig. 7i).

4 Discussion

In our study, we proved that LIPUS could ameliorate AngII-stimulated cardiac fibrosis via increased expression of the mechano-transduction protein caveolin-1. We speculated that caveolin-1 might play a possible role during the pathological process of cardiac fibrosis induced by AngII administration. To our knowledge, this study demonstrates for the first time that LIPUS irradiation can improve AngII-induced cardiac fibrosis by alleviating inflammation via a caveolin-1-dependent pathway.

As a well-recognized octameric peptide hormone in the RAS, AngII has been identified to promote fibroblast differentiation in a hemodynamics-dependent or -independent manner by interacting with the type 1 angiotensin (AT1) receptor (Gebremichael et al., 2019). The activated differentiation of cardiac fibroblasts to myofibroblasts is characterized as the hallmark of cardiac fibrosis and is essential in enhancing mechanical

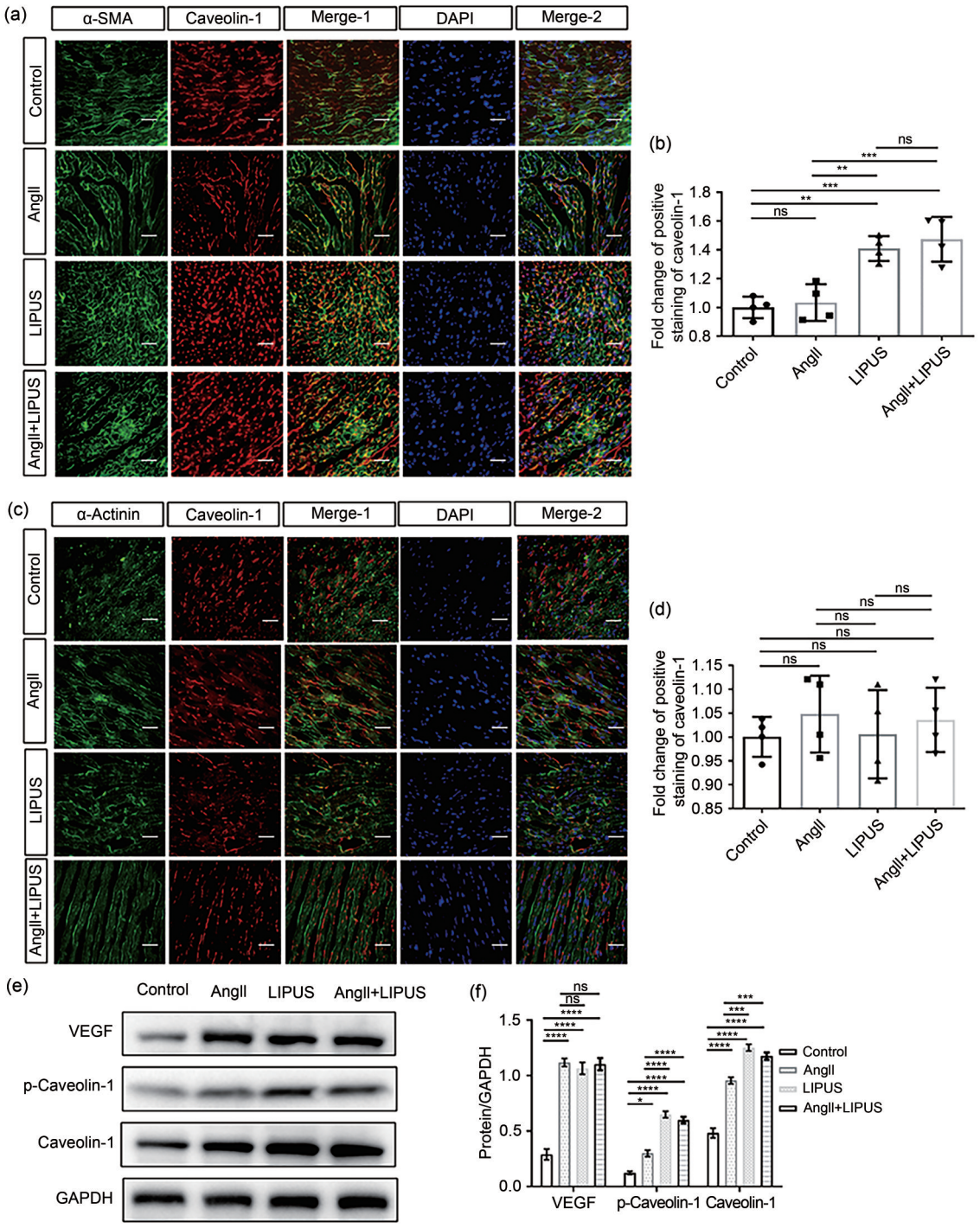

Fig. 4 Involvement of caveolin-1 in the effects of LIPUS on ameliorating AngII-stimulated cardiac hypertrophy in mice. (a, b) The paraffin sections of LV tissues (a) labeled with caveolin-1, α-SMA, and DAPI (caveolin-1, red; α-SMA, green; DAPI, blue; scale bar=50 μm) and their quantitative analyses (b). (c, d) The paraffin sections of LV tissues (c) labeled with caveolin-1, α-actinin, and DAPI (caveolin-1, red; α-actinin, green; DAPI, blue; scale bar=50 μm) and their quantitative analyses (d). (e, f) Protein levels of phospho-caveolin-1 (p-caveolin-1), caveolin-1, and VEGF in isolated mice hearts from the indicated groups (e) and their densitometric analyses (f). Results are presented as mean±standard error of the mean (SEM), n>3 per group. ns indicates being not significant; * P<0.05, ** P<0.01, *** P<0.001, **** P<0.0001. LIPUS, low-intensity pulsed ultrasound; AngII, angiotensin II; LV, left ventricle; α-SMA, α-smooth muscle actin; DAPI, 4',6-diamidino-2-phenylindole; VEGF, vascular endothelial growth factor; GAPDH, glyceraldehyde-3-phosphate dehydrogenase.

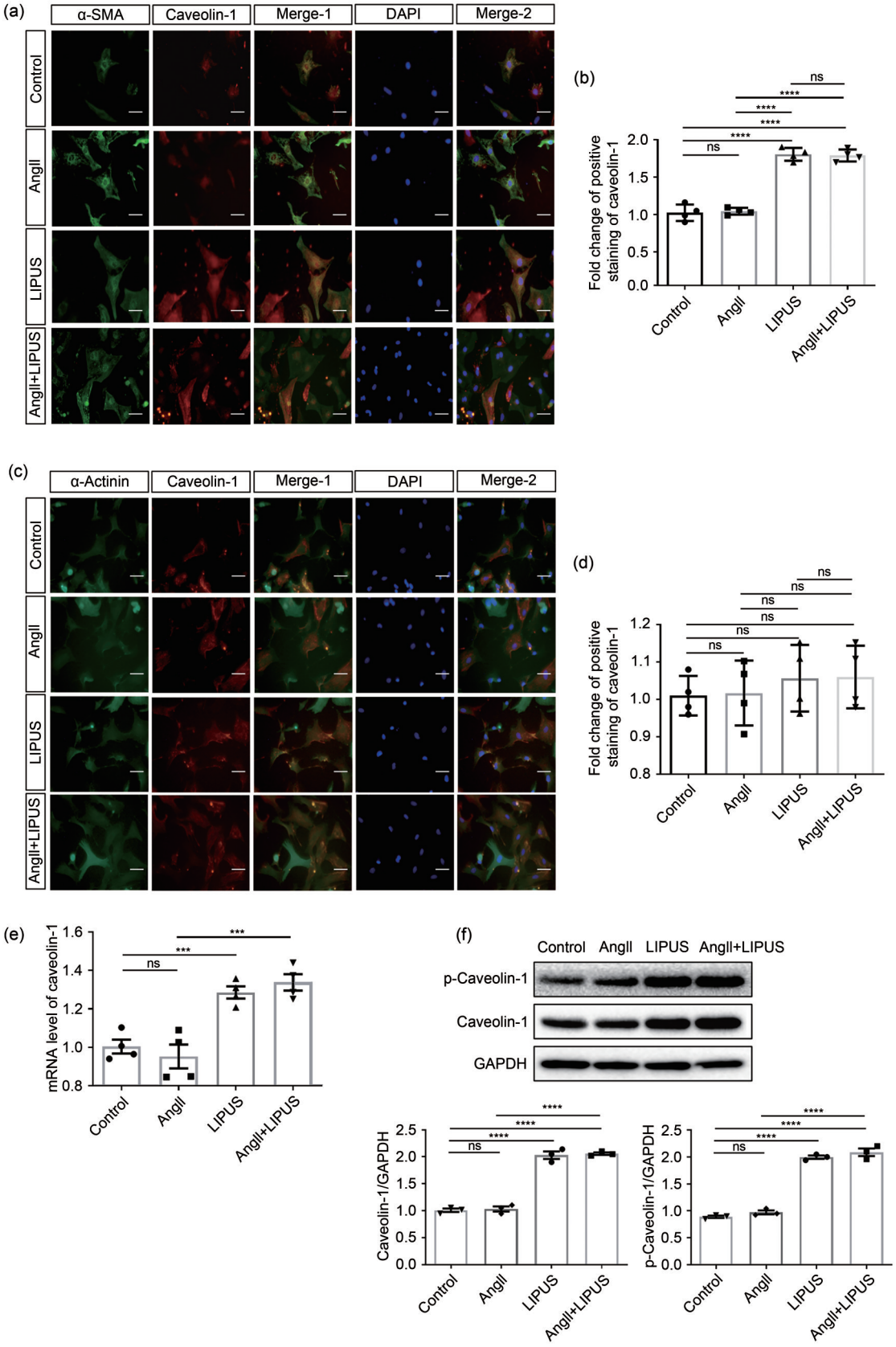
(a)
α-SMA
Caveolin-1
Merge-1
DAPI
Merge-2
Control
AngII
LIPUS
AngII+LIPUS
(b)
Fold change of positive staining of caveolin-1
ns
****
Control
AngII
LIPUS
AngII+LIPUS
(c)
α-Actinin
Caveolin-1
Merge-1
DAPI
Merge-2
Control
AngII
LIPUS
AngII+LIPUS
(d)
Fold change of positive staining of caveolin-1
ns
Control
AngII
LIPUS
AngII+LIPUS
(e)
mRNA level of caveolin-1
ns
***
Control
AngII
LIPUS
AngII+LIPUS
(f)
Control
AngII
LIPUS
AngII+LIPUS
p-Caveolin-1
Caveolin-1
GAPDH
Caveolin-1/GAPDH
p-Caveolin-1/GAPDH
ns
****
Control
AngII
LIPUS
AngII+LIPUS

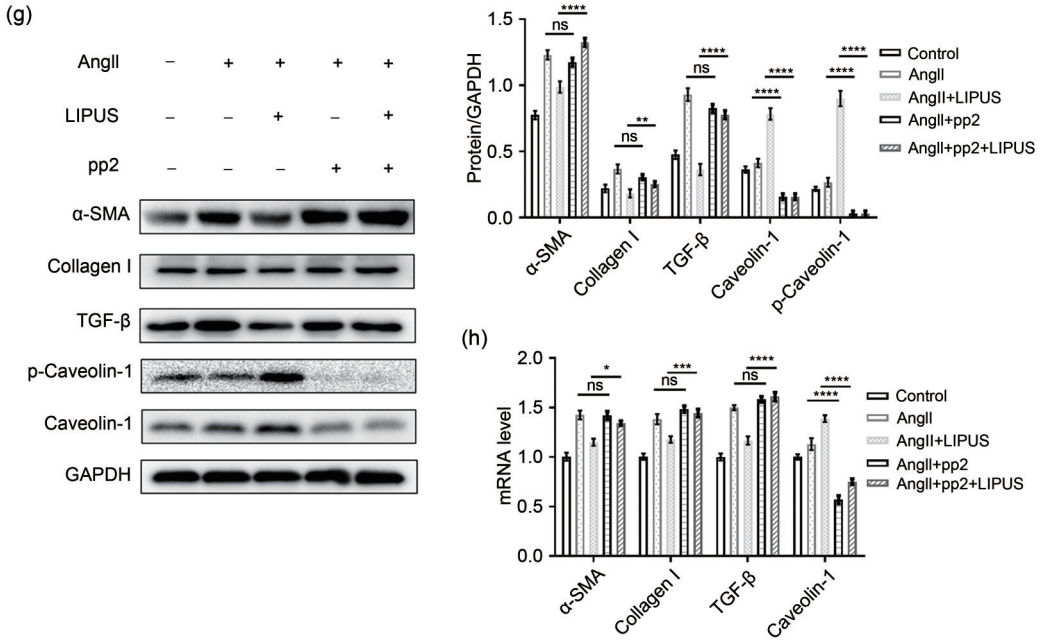

Fig. 5 Involvement of caveolin-1 in the effects of LIPUS on ameliorating AngII-stimulated cardiac fibrosis in vitro. (a, b) The NRCFs (a) labeled with caveolin-1, α-SMA, and DAPI (caveolin-1, red; α-SMA, green; DAPI, blue; scale bar=50 μm) and their quantitative analyses (b). (c, d) The cardiomyocytes (c) labeled with caveolin-1, α-actinin, and DAPI (caveolin-1, red; α-actinin, green; DAPI, blue; scale bar=50 μm) and their quantitative analyses (d). (e, f) mRNA (e) and protein (f) expression levels of p-caveolin-1 and caveolin-1 in NRCFs from indicated groups. (g, h) Protein (g) and mRNA (h) expression levels of phospho-caveolin-1 (p-caveolin-1), caveolin-1, α-SMA, TGF-β, and collagen I in NRCFs from the control group, the model groups with/without pp2 pretreatment, and the LIPUS treatment groups with/without pp2 pretreatment and their densitometric analyses. Results are presented as mean±standard error of the mean (SEM), n>3 per group. ns indicates being not significant; * P<0.05, ** P<0.01, *** P<0.001, **** P<0.0001. LIPUS, low-intensity pulsed ultrasound; AngII, angiotensin II; NRCF, neonatal rat cardiac fibroblast; α-SMA, α-smooth muscle actin; DAPI, 4',6-diamidino-2-phenylindole; TGF-β, transforming growth factor β; pp2, pyrazolopyrimidine 2; GAPDH, glyceraldehyde-3-phosphate dehydrogenase.

stability through increasing collagen secretion and α-SMA expression during cardiac remodeling (Nguyen et al., 2014). The continuous accumulation of α-SMA-expressing myofibroblasts may result in excessive deposition and remodeling of the ECM (She et al., 2019). Additionally, injury to the left ventricular structure and function and activation of fetal genes including *ANP*, *BNP*, *α-MHC*, and *β-MHC* are observed in cardiac hypertrophy and are crucial pathological changes during the progression of cardiac remodeling (Yan et al., 2017).

LIPUS, a novel ultrasonic therapy technique, was reported to exert its biological effects in fracture healing and tumor treatment without tissue compression, overheating, or other side effects (Jiang et al., 2019). Recently, LIPUS irradiation has been reported to suppress myocardial fibrosis induced by acute MI in animal models (Zheng et al., 2019). Therefore, further investigations were performed to confirm whether LIPUS irradiation could ameliorate AngII-induced cardiac hypertrophy and fibrosis.

In our study, we treated AngII-stimulated rat cardiomyocytes and cardiac fibroblasts with/without LIPUS irradiation in vitro. Under the premise that ultrasound stimulation has no effect on cell apoptosis, the obtained molecular biological and immunofluorescence revealed that LIPUS could inhibit the differentiation of cardiac fibroblasts to myofibroblasts and the activation of fetal genes associated with cardiac hypertrophy, except *α-MHC* and *β-MHC*, in cell culture models. LIPUS irradiation slightly inhibited AngII-induced hypertrophic growth of cardiomyocytes in our study, suggesting that LIPUS has a beneficial effect on AngII-induced cardiac fibrosis that is limited to cardiac hypertrophy in vitro. Since cardiomyocytes undergo sustained electrical and mechanical activity, which is important for normal contraction-relaxation cycles (Saucerman et al., 2019), we supposed that cardiac

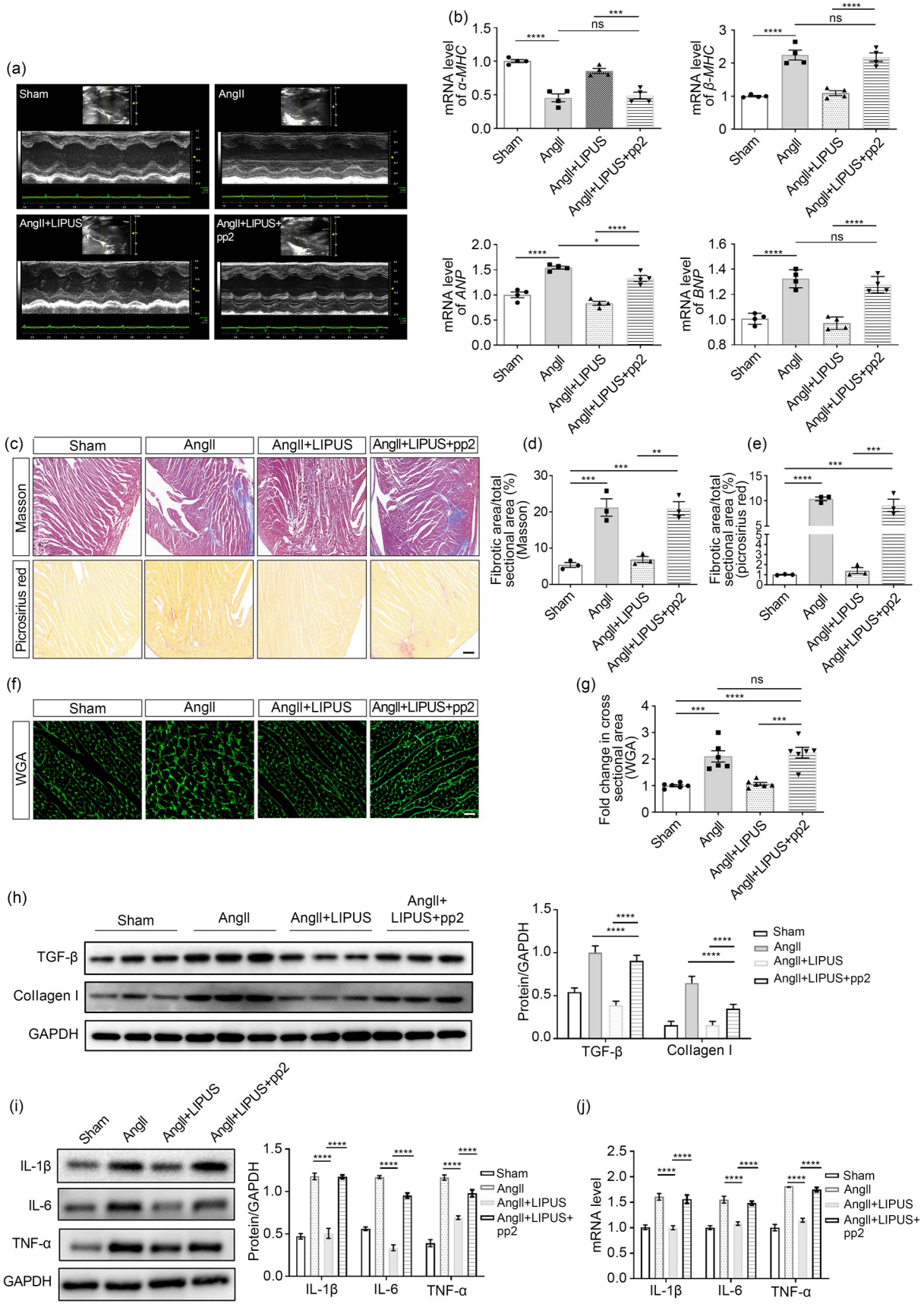
(a)
Sham
AngII
AngII+LIPUS
AngII+LIPUS+pp2
(b)
mRNA level of α-MHC
mRNA level of β-MHC
mRNA level of ANP
mRNA level of BNP
Sham
AngII
AngII+LIPUS
AngII+LIPUS+pp2
ns
(c)
Masson
Picrosirius red
(d)
Fibrotic area/total sectional area (%) (Masson)
(e)
Fibrotic area/total sectional area (%) (picrosirius red)
(f)
WGA
(g)
Fold change in cross sectional area (WGA)
(h)
TGF-β
Collagen I
GAPDH
Protein/GAPDH
(i)
IL-1β
IL-6
TNF-α
GAPDH
(j)
mRNA level

Fig. 6 Involvement of caveolin-1 in the effects of LIPUS on ameliorating AngII-stimulated cardiac fibrosis in vitro. (a) Representative M-mode echocardiography images of the hearts from the sham group (*n*=5), AngII group (*n*=8), AngII+ LIPUS group (*n*=8), and AngII+LIPUS+pp2 group (*n*=5). (b) mRNA levels of fetal genes in isolated mice hearts from indicated groups. (c) The longitudinal sections of LV tissues stained with Masson's method (scale bar=200 μm) and picrosirius red (scale bar=200 μm) from indicated groups. (d, e) Quantitative analyses of collagen deposition stained with Masson's method (d) and picrosirius red (e). (f) The longitudinal sections of LV tissues stained with wheat germ agglutinin (WGA; scale bar=50 μm) from indicated groups. (g) Quantitative analyses of the cardiomyocyte cross-sectional areas stained with WGA. At least 50 cardiomyocytes per group were measured randomly using Image-Pro Plus software. (h, i) Protein expression levels of TGF-β, collagen I (h), IL-1β, IL-6, and TNF-α (i) in frozen mice heart samples from different groups and their corresponding densitometric analyses. (j) mRNA levels of IL-1β, IL-6, and TNF-α in NRCFs from indicated groups. Results are presented as mean±standard error of the mean (SEM), *n*>3 per group. ns indicates being not significant; * *P*<0.05, ** *P*<0.01, * *P*<0.001, **** *P*<0.0001. LIPUS, low-intensity pulsed ultrasound; AngII, angiotensin II; pp2, pyrazolopyrimidine 2; LV, left ventricle; TGF-β, transforming growth factor β; IL, interleukin; TNF-α, tumor necrosis factor-α; NRCF, neonatal rat cardiac fibroblast; *ANP*, atrial natriuretic peptide; *BNP*, B-type natriuretic peptide; *MHC*, myosin heavy chain; GAPDH, glyceraldehyde-3-phosphate dehydrogenase.**

Table 2 Echocardiographic data of left ventricular function at the end of four weeks

Group	LVEF (%)	LVFS (%)	LVIDd (mm)	LVIDs (mm)	LVESV (mm)	MAPSE (mm)
Sham	72.100±1.646	40.100±1.338	3.130±0.050	1.876±0.059	10.890±0.878	0.661±0.025
AngII	47.920±1.970*	23.590±1.199*	3.631±0.060*	2.773±0.054*	28.940±1.381*	0.467±0.011*
AngII+LIPUS	65.160±1.021	34.440±0.709	2.970±0.066	1.948±0.059	11.990±0.952	0.619±0.017
AngII+LIPUS+pp2	56.590±1.931#	28.940±1.267#	3.505±0.098#	2.494±0.100#	23.940±2.133#	0.531±0.016#

The results are presented as mean±standard error of the mean (SEM), *n*>3 per group. * *P*<0.05 vs. the sham group; # *P*<0.05 vs. the AngII+LIPUS group. AngII, angiotensin II; LIPUS, low-intensity pulsed ultrasound; pp2, pyrazolopyrimidine 2; LVEF, left ventricular ejection fraction; LVFS, left ventricular fractional shortening; LVIDd, left ventricular internal diameters at end diastole; LVIDs, left ventricular internal diameters at end systole; LVESV, left ventricle end-systolic volume; MAPSE, mitral annular plane systolic excursion.

fibroblasts may be more sensitive to mechanical stimulation derived from LIPUS than cardiomyocytes. This may account for why LIPUS irradiation could ameliorate AngII-induced cardiac fibrosis, but not cardiac hypertrophy in vitro. Furthermore, we mimicked AngII-induced cardiac remodeling in a mouse model using an ALZET 2004 osmotic mini-pump filled with AngII in vivo. The model was formed after chronic AngII infusion for four weeks, while models that did not form successfully at the end of the two weeks were analyzed using echocardiographic data (Table S3). The treatment group received LIPUS irradiation for 20 min every 2 d from one week before mini-pump implantation to four weeks after mini-pump implantation. As expected, our echocardiographic and histopathological data and molecular biological results revealed that LIPUS irradiation ameliorated AngII-stimulated cardiac structural and hemodynamic changes associated with cardiac hypertrophy and alleviated myocardial fibrosis in vivo. Unlike newborn hearts, 60%–70% of cells in adult hearts are cardiac fibroblasts that play essential roles in maintaining standard heart structure, repairing a damaged heart, and transmitting mechanical and electrical signals (Porter and Turner, 2009; Tallquist, 2020). Regarding the different effects of LIPUS on cardiac hypertrophy in vivo and in vitro, we suggested that the ameliorated cardiac fibrosis contributes to the improved cardiac hypertrophy in vivo.

Previous studies demonstrated that impaired cardiac systolic function can be indicated by several parameters, including LVESV, LVEF, MAPSE, and global longitudinal LV strain (GLS) (Ribeiro et al., 2019; Hendriks et al., 2020). MAPSE and GLS were reported to have superior prognostic value to LVEF for predicting cardiac systolic function (Kalam et al., 2014; Ribeiro et al., 2019). GLS was reported to be a more sensitive measure of systolic function, but its measurement requires special ultrasound techniques, which we lack. Thus, we used M-mode echocardiography to measure MAPSE in the apical four-chamber views. Besides, we provided the values of LVEF and LVESV. A previous study found that LIPUS could ameliorate cardiac diastolic dysfunction in db/db mice (Monma et al., 2021). In our study, the values of MAPSE, LVEF, LVFS, and LVESV showed that LIPUS irradiation could not only improve cardiac fibrosis, but also ameliorate AngII-induced cardiac diastolic dysfunction. LIPUS has been reported to exert several biological effects by mechanical stimulation related to caveolae and caveolin-1. In addition to regulating signal transduction between caveolar and non-caveolar regions, caveolae composed of a subset of lipid (membrane) rafts have been shown to

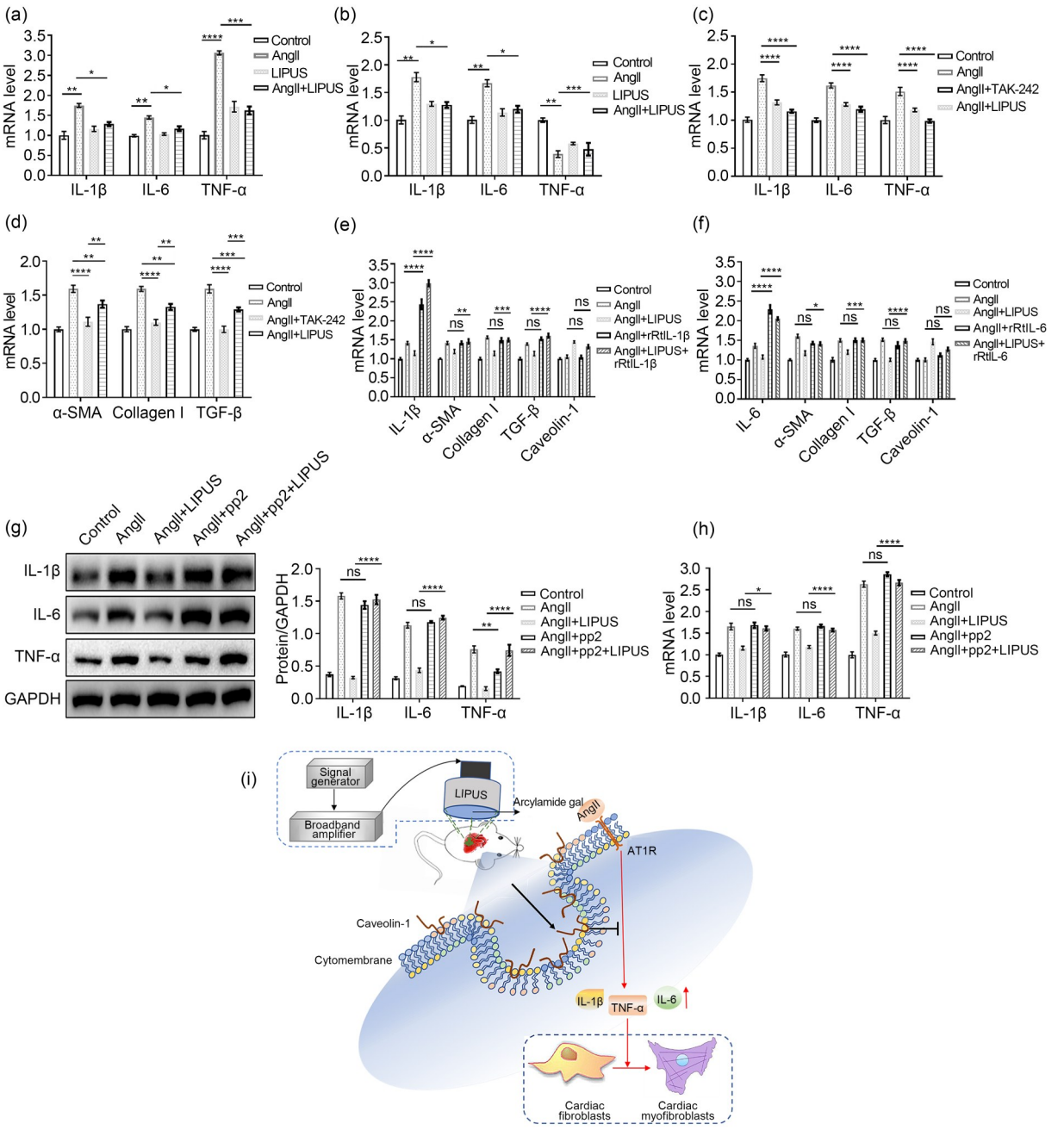

Fig. 7 Relationship between inflammation and caveolin-1 in the anti-fibrotic effects of LIPUS irradiation in vivo. (a, b) mRNA levels of IL-1β, IL-6, and TNF-α in NRCFs (a) and frozen mice hearts (b) from the indicated groups. (c, d) mRNA levels of IL-1β, IL-6, TNF-α, α-SMA, TGF-β, and collagen I in NRCFs from the control group, the model groups with/without TAK-242 pretreatment, and the LIPUS treatment groups. (e, f) mRNA expression levels of IL-6, caveolin-1, α-SMA, TGF-β, and collagen I in NRCFs from the control group, the model groups with/without rRtIL-1β/ rRtIL-6 pretreatment, and the LIPUS treatment groups with/without rRtIL-1β/rRtIL-6 pretreatment. (g, h) Protein (g) and mRNA (h) expression levels of IL-1β, IL-6, and TNF-α in cardiac fibroblasts from the control group, the model groups with/without pp2 pretreatment, and the LIPUS treatment groups with/without pp2 pretreatment. (i) Possible molecular mechanisms for the therapeutic effects of LIPUS are shown. Results are presented as mean±standard error of the mean (SEM), *n*>3 per group. ns indicates being not significant; * *P*<0.05, ** *P*<0.01, * *P*<0.001, **** *P*<0.0001. LIPUS, low-intensity pulsed ultrasound; IL, interleukin; TNF-α, tumor necrosis factor-α; NRCF, neonatal rat cardiac fibroblast; α-SMA, α-smooth muscle actin; TGF-β, transforming growth factor-β; rRtIL, recombinant rat interleukin; pp2, pyrazolopyrimidine 2; GAPDH, glyceraldehyde-3-phosphate dehydrogenase; AngII, angiotensin II.**

respond and adapt to environmental perturbations in various physiopathologic processes (Parton et al., 2018). Caveolin-1, a crucial integral membrane protein within caveolar membranes, can interact with and sequester various membrane signaling molecules in tissue remodeling by binding to the caveolin-1 scaffolding domain (Vogel et al., 2019; Volonte and Galbiati, 2020). Given that cyclic mechanical stretch can reduce myofibroblast differentiation, caveolin-1 has been studied as a novel therapeutic target of fibrosis (Shihata et al., 2017; Marudamuthu et al., 2019). Previous reports have shown that caveolin-1 plays an antifibrotic role in negative regulation of ECM remodeling through coordinating cytoskeletal rearrangement, cell directional migration, and apoptosis (Nethe and Hordijk, 2011; Chung et al., 2018). Due to its role in modulating TGF-β1 signaling via downregulated expression of collagen I and other proproinflammatory cytokines, caveolin-1 has also been identified to interact and interfere with the function of the TGF-β receptor (Razani et al., 2001). Restoring or reintroduction of caveolin-1 expression has been shown to attenuate and prevent fibrotic diseases induced by fibrotic agents such as TGF-β1 (Gvaramia et al., 2013; Liu et al., 2015). However, the possible role of caveolin-1 in the treatment of LIPUS irradiation for AngII-stimulated cardiac fibrosis was still unclear. Here, we found that LIPUS irradiation increased the expression of caveolin-1 in vivo and in vitro. Except that LIPUS itself can increase the expression of caveolin-1 by mechanical stimulation, there was no difference in caveolin-1 expression in cardiac fibroblasts between the control group and the model group. In addition, post-translational modifications of caveolin-1, specifically its tyrosine-14 residue phosphorylation (pY14-Cav1), have been found to play a vital role in fibrotic diseases (Gvaramia et al., 2013; Buwa et al., 2020). In a previous study, a link was found between LIPUS irradiation and the activation of caveolin-1 (Zheng et al., 2019). In our study, LIPUS irradiation promoted the pY14-Cav1 of caveolin-1, and the reversal study indicated that LIPUS-stimulated pY14-Cav1 contributed to the antifibrotic effects of LIPUS irradiation on AngII-stimulated cardiac fibrosis (Fig. S6a). However, caveolin-1 expression in the model group was significantly higher than that in the control group in frozen heart tissues. VEGF is crucial in compensated angiogenesis associated with maintaining cardiac function (Zaragoza et al., 2021). AngII and LIPUS irradiation have been reported to induce endothelium-derived angiogenesis by different mechanisms (Shindo et al., 2016; Chen et al., 2019), which may support our finding of increased protein expression of VEGF in mice hearts after AngII and/or LIPUS treatment. Given that caveolin-1 is highly expressed in the endothelium (Ito et al., 2019), the above reasons may explain the increased caveolin-1 expression in heart tissues in the model group. After pretreatment with the caveolin-1 inhibitor pp2 both in vivo and in vitro, the protective effects of LIPUS against AngII-induced cardiac fibrosis were all reversed, suggesting the role of caveolin-1 in LIPUS irradiation.

Also, we evaluated the blood pressure (BP) in animal models. First, LIPUS irradiation downregulated the AngII-induced increase of systolic blood pressure (SBP) and mean blood pressure (MBP), but not diastolic blood pressure (DBP) at two weeks after AngII infusion (Figs. S7a−S7c). Though caveolin-1 has an important role in controlling central BP variability, previous studies have found that there was no difference in SBP between WT and cavonlin-1 knockout (KO) mice (Desjardins et al., 2008; Swärd et al., 2014). A similar trend was also found in our study. The results showed that pp2 treatment, which downregulated caveolin-1 expression, did not reverse the effects of LIPUS on lowering SBP and MBP in vivo, suggesting that LIPUS may exert its antifibrotic effects independent of BP. Since BP had not been the focus of our attention, we measured BP only three times after LIPUS irradiation. We supposed that there are other mechanisms that could explain the possible effect of LIPUS on lowering SBP, and this needs to be further investigated.

AngII-induced cardiac remodeling is characterized by a pathophysiological response to chronic inflammation with progressive fibrosis (Zhao et al., 2019; Lin et al., 2021). In this process, an inflammatory milieu can promote the phenotypic transformation of cardiac fibroblasts (Ji et al., 2020). AngII is known to have a strong proinflammatory and reported profibrotic effects on facilitating the synthesis of ECM and further contributing to myocardial fibrosis with increased expression of cytokines such as IL-1β, IL-6, and TNF-α (She et al., 2019).

It remained to be seen whether LIPUS irradiation could exert its effects on AngII-induced cardiac fibrosis by regulating the inflammatory response. In our study, LIPUS irradiation reduced AngII-induced release of

proinflammatory cytokines in vivo and in vitro, and overexpression of both IL-1β and IL-6 reversed the antifibrotic effects of LIPUS irradiation. This supports the suggestion that LIPUS attenuates cardiac fibrosis following AngII administration by alleviating inflammation in vitro. Furthermore, administration of pp2 downregulated the expression of proinflammatory cytokines in vivo and in vitro, while the use of rRtIL-1β or rRtIL-6 did not affect the expression of caveolin-1. AngII stimulation may evoke a primary M1 pro-inflammatory response and a subsequent M2 fibrotic response, thereby contributing to the occurrence and progression of fibrotic diseases (Duerrschmid et al., 2015). Cluster of differentiation 68 (CD68) is a marker for macrophage lineage cells, and the infiltration of CD68-positive macrophages plays a vital role during cardiac fibrosis (González et al., 2016). Here, we examined CD68 cell infiltration by detecting protein and mRNA expression, as well as the immunofluorescence intensity of CD68 in heart tissues from different groups in vivo. The results showed that LIPUS irradiation inhibited AngII-induced CD68 infiltration of cell membranes, and pp2 pretreatment could reverse this effect (Figs. S8a–S8c). These results suggested that in addition to inflammation, the activation of immune cells represented by CD68 infiltration may be involved in the antifibrotic effects of LIPUS irradiation.

Since LIPUS has been reported to have a protective effect against oxidative stress on endothelial-mesenchymal transition (Li et al., 2018), we evaluated the role of oxidative stress in the cardioprotective effects of LIPUS. First, we found that LIPUS irradiation downregulated AngII-induced LDH, SOD, and MDA concentrations in cardiac fibroblasts when compared to the control group (Figs. S9a–S9c). Then, we used the reactive oxygen species (ROS) scavenger *N*-acetylcysteine and the ROS producing agent *tert*-butyl hydroperoxide (tBHP) for further experiments in vitro. The data indicated that *N*-acetylcysteine could mimic or even enhance the anti-fibrotic effect of LIPUS irradiation (Fig. S9d), whereas tBHP reversed this effect (Fig. S9e), but the underlying mechanism remains to be further investigated.

Taken together, we have partly explained the therapeutic value of LIPUS irradiation in AngII-induced cardiac fibrosis (Fig. 6h). However, there are some limitations that need to be considered. First, compared with its effects in vivo, the beneficial effects of LIPUS irradiation on cardiac hypertrophy were rather small in cardiomyocytes. We speculated that more irradiation sessions in vivo may enhance the protective effects of LIPUS, since the cardiomyocytes may be less sensitive than cardiac fibroblasts to mechanical stimulation derived from LIPUS. Second, we have not examined whether the effects of LIPUS irradiation observed in our study may be blunted in caveolin-1 knockdown mice. Third, regarding the molecular mechanisms, in this study we focused mainly on the caveolin-1-mediated inflammatory response. As several reports have shown that MAPK and other signaling pathways are closely related to LIPUS-induced biological effects, these remain to be further studied in relation to the antifibrotic role of LIPUS irradiation (Ren et al., 2013; Zheng et al., 2019).

5 Conclusions

This study sheds light on the protective effects of LIPUS irradiation on ameliorating AngII-induced cardiac fibrosis by alleviating inflammation via a caveolin-1-dependent pathway. Therefore, LIPUS irradiation may be considered a safe and noninvasive therapy for prevention of cardiac fibrosis in future clinical applications.

Acknowledgments

This work was supported by the National Natural Science Foundation of China (No. 81627802), the Priority Academic Program Development of Jiangsu Higher Education Institutions (No. PAPD2014-2016), and the National Key R&D Program of China (No. 2019YFA0210100).

Author contributions

Kun ZHAO performed the experimental research and contributed to the study design, wrote and edited the manuscript. Jing ZHANG performed the establishment of animal models, wrote and edited the manuscript. Tianhua XU contributed to the study design. Chuanxi YANG and Xiaoguang WU contributed to the data analysis. Liqing WENG and Tingting WU contributed to the establishment of animal models. Jiaming MIAO, Xiasheng GUO, Juan TU, Dong ZHANG, and Xiangqing KONG contributed to the design and build of LIPUS. Bin ZHOU, Wei SUN, and Xiangqing KONG edited the manuscript. All authors have read and approved the final manuscript and, therefore, have full access to all the data in the study and take responsibility for the integrity and security of the data.

Compliance with ethics guidelines

Kun ZHAO, Jing ZHANG, Tianhua XU, Chuanxi YANG, Liqing WENG, Tingting WU, Xiaoguang WU, Jiaming MIAO, Xiasheng GUO, Juan TU, Dong ZHANG, Bin ZHOU, Wei SUN, and Xiangqing KONG declare that they have no conflict of interest.

All experiments with animals were conducted strictly following the University's guidelines for the Care and Use of Laboratory Animals (Publication No. 85-23, Revised 1996; National Institutes of Health, Bethesda, MD, USA) and were approved by the Committee on Use and Care of Experimental Animals of Nanjing Medical University (Nanjing, China).

References

Ames MK, Atkins CE, Pitt B, 2019. The renin-angiotensin-aldosterone system and its suppression. *J Vet Intern Med*, 33(2):363-382. https://doi.org/10.1111/jvim.15454

Buwa N, Mazumdar D, Balasubramanian N, 2020. Caveolin1 tyrosine-14 phosphorylation: role in cellular responsiveness to mechanical cues. *J Membr Biol*, 253(6):509-534. https://doi.org/10.1007/s00232-020-00143-0

Chen LY, Wang X, Qu XL, et al., 2019. Activation of the STAT3/microRNA-21 pathway participates in angiotensin II-induced angiogenesis. *J Cell Physiol*, 234(11):19640-19654. https://doi.org/10.1002/jcp.28564

Chinnakkannu P, Reese C, Gaspar JA, et al., 2018. Suppression of angiotensin II-induced pathological changes in heart and kidney by the caveolin-1 scaffolding domain peptide. *PLoS ONE*, 13(12):e0207844. https://doi.org/10.1371/journal.pone.0207844

Chung JW, Kim DH, Oh MJ, et al., 2018. Cav-1 (caveolin-1) and arterial remodeling in adult moyamoya disease. *Stroke*, 49(11):2597-2604. https://doi.org/10.1161/strokeaha.118.021888

Desjardins F, Lobysheva I, Pelat M, et al., 2008. Control of blood pressure variability in caveolin-1-deficient mice: role of nitric oxide identified *in vivo* through spectral analysis. *Cardiovasc Res*, 79(3):527-536. https://doi.org/10.1093/cvr/cvn080

Ding L, Zeng QM, Wu JP, et al., 2017. Caveolin-1 regulates oxidative stress-induced senescence in nucleus pulposus cells primarily via the p53/p21 signaling pathway in vitro. *Mol Med Rep*, 16(6):9521-9527. https://doi.org/10.3892/mmr.2017.7789

Duerrschmid C, Trial J, Wang YL, et al., 2015. Tumor necrosis factor: a mechanistic link between angiotensin-II-induced cardiac inflammation and fibrosis. *Circ Heart Fail*, 8(2):352-361. https://doi.org/10.1161/circheartfailure.114.001893

Forrester SJ, Elliott KJ, Kawai T, et al., 2017. Caveolin-1 deletion prevents hypertensive vascular remodeling induced by angiotensin II. *Hypertension*, 69(1):79-86. https://doi.org/10.1161/hypertensionaha.116.08278

Frangogiannis NG, 2021. Cardiac fibrosis. *Cardiovasc Res*, 117(6):1450-1488. https://doi.org/10.1093/cvr/cvaa324

Gebremichael Y, Lahu G, Vakilynejad M, et al., 2019. Benchmarking renin suppression and blood pressure reduction of direct renin inhibitor imarikiren through quantitative systems pharmacology modeling. *J Pharmacokinet Pharmacodyn*, 46(1):15-25. https://doi.org/10.1007/s10928-018-9612-y

González GE, Rhaleb NE, D'Ambrosio MA, et al., 2016. Cardiac-deleterious role of galectin-3 in chronic angiotensin II-induced hypertension. *Am J Physiol Heart Circ Physiol*, 311(5):H1287-H1296. https://doi.org/10.1152/ajpheart.00096.2016

Grivas D, González-Rajal Á, Rodríguez CG, et al., 2020. Loss of Caveolin-1 and caveolae leads to increased cardiac cell stiffness and functional decline of the adult zebrafish heart. *Sci Rep*, 10:12816. https://doi.org/10.1038/s41598-020-68802-9

Gvaramia D, Blaauboer ME, Hanemaaijer R, et al., 2013. Role of caveolin-1 in fibrotic diseases. *Matrix Biol*, 32(6):307-315. https://doi.org/10.1016/j.matbio.2013.03.005

Hanna A, Frangogiannis NG, 2020. Inflammatory cytokines and chemokines as therapeutic targets in heart failure. *Cardiovasc Drugs Ther*, 34(6):849-863. https://doi.org/10.1007/s10557-020-07071-0

Hendriks T, van Dijk R, Alsabaan NA, et al., 2020. Active tobacco smoking impairs cardiac systolic function. *Sci Rep*, 10:6608. https://doi.org/10.1038/s41598-020-63509-3

Ito A, Shiroto T, Godo S, et al., 2019. Important roles of endothelial caveolin-1 in endothelium-dependent hyperpolarization and ischemic angiogenesis in mice. *Am J Physiol Heart Circ Physiol*, 316(4):H900-H910. https://doi.org/10.1152/ajpheart.00589.2018

Ji JJ, Liu ZF, Hong XX, et al., 2020. Protective effects of rolipram on endotoxic cardiac dysfunction via inhibition of the inflammatory response in cardiac fibroblasts. *BMC Cardiovasc Disord*, 20:242. https://doi.org/10.1186/s12872-020-01529-7

Jiang XX, Savchenko O, Li YF, et al., 2019. A review of low-intensity pulsed ultrasound for therapeutic applications. *IEEE Trans Biomed Eng*, 66(10):2704-2718. https://doi.org/10.1109/tbme.2018.2889669

Jokhadar ŠZ, Majhenc J, Svetina S, et al., 2013. Positioning of integrin β1, caveolin-1 and focal adhesion kinase on the adhered membrane of spreading cells. *Cell Biol Int*, 37(12):1276-1284. https://doi.org/10.1002/cbin.10155

Kalam K, Otahal P, Marwick TH, 2014. Prognostic implications of global LV dysfunction: a systematic review and meta-analysis of global longitudinal strain and ejection fraction. *Heart*, 100(21):1673-1680. https://doi.org/10.1136/heartjnl-2014-305538

Lennmyr F, Ericsson A, Gerwins P, et al., 2004. Src family kinase-inhibitor PP2 reduces focal ischemic brain injury. *Acta Neurol Scand*, 110(3):175-179. https://doi.org/10.1111/j.1600-0404.2004.00306.x

Li J, Zhang Q, Ren C, et al., 2018. Low-intensity pulsed ultrasound prevents the oxidative stress induced

endothelial-mesenchymal transition in human aortic endothelial cells. *Cell Physiol Biochem*, 45(4):1350-1365. https://doi.org/10.1159/000487561

Lin YM, Badrealam KF, Kuo WW, et al., 2021. Nerolidol improves cardiac function in spontaneously hypertensive rats by inhibiting cardiac inflammation and remodelling associated TLR4/NF-κB signalling cascade. *Food Chem Toxicol*, 147:111837. https://doi.org/10.1016/j.fct.2020.111837

Liu JJ, Song C, Xiao QM, et al., 2015. Fluorofenidone attenuates TGF-β1-induced lung fibroblast activation via restoring the expression of caveolin-1. *Shock*, 43(2):201-207. https://doi.org/10.1097/shk.0000000000000273

Ma ZG, Yuan YP, Wu HM, et al., 2018. Cardiac fibrosis: new insights into the pathogenesis. *Int J Biol Sci*, 14(12): 1645-1657. https://doi.org/10.7150/ijbs.28103

Marudamuthu AS, Bhandary YP, Fan L, et al., 2019. Caveolin-1-derived peptide limits development of pulmonary fibrosis. *Sci Transl Med*, 11(522):eaat2848. https://doi.org/10.1126/scitranslmed.aat2848

Monma Y, Shindo T, Eguchi K, et al., 2021. Low-intensity pulsed ultrasound ameliorates cardiac diastolic dysfunction in mice: a possible novel therapy for heart failure with preserved left ventricular ejection fraction. *Cardiovasc Res*, 117(5):1325-1338. https://doi.org/10.1093/cvr/cvaa221

Nakamura M, Sadoshima J, 2018. Mechanisms of physiological and pathological cardiac hypertrophy. *Nat Rev Cardiol*, 15(7):387-407. https://doi.org/10.1038/s41569-018-0007-y

Nethe M, Hordijk PL, 2011. A model for phospho-caveolin-1-driven turnover of focal adhesions. *Cell Adh Migr*, 5(1): 59-64. https://doi.org/10.4161/cam.5.1.13702

Nguyen TP, Qu ZL, Weiss JN, 2014. Cardiac fibrosis and arrhythmogenesis: the road to repair is paved with perils. *J Mol Cell Cardiol*, 70:83-91. https://doi.org/10.1016/j.yjmcc.2013.10.018

Ogata T, Ito K, Shindo T, et al., 2017. Low-intensity pulsed ultrasound enhances angiogenesis and ameliorates contractile dysfunction of pressure-overloaded heart in mice. *PLoS ONE*, 12(9):e0185555. https://doi.org/10.1371/journal.pone.0185555

Parton RG, Tillu VA, Collins BM, 2018. Caveolae. *Curr Biol*, 28(8):R402-R405. https://doi.org/10.1016/j.cub.2017.11.075

Porter KE, Turner NA, 2009. Cardiac fibroblasts: at the heart of myocardial remodeling. *Pharmacol Ther*, 123(2):255-278. https://doi.org/10.1016/j.pharmthera.2009.05.002

Razani B, Zhang XL, Bitzer M, et al., 2001. Caveolin-1 regulates transforming growth factor (TGF)-β/SMAD signaling through an interaction with the TGF-β type I receptor. *J Biol Chem*, 276(9):6727-6738. https://doi.org/10.1074/jbc.M008340200

Ren LX, Yang Z, Song JL, et al., 2013. Involvement of p38 MAPK pathway in low intensity pulsed ultrasound induced osteogenic differentiation of human periodontal ligament cells. *Ultrasonics*, 53(3):686-690. https://doi.org/10.1016/j.ultras.2012.10.008

Ribeiro S, Pereira ARS, Pinto AT, et al., 2019. Echocardiographic assessment of cardiac anatomy and function in adult rats. *J Vis Exp*, 154:e60404. https://doi.org/10.3791/60404

Rosenkranz S, 2004. TGF-β1 and angiotensin networking in cardiac remodeling. *Cardiovasc Res*, 63(3):423-432. https://doi.org/10.1016/j.cardiores.2004.04.030

Saucerman JJ, Tan PM, Buchholz KS, et al., 2019. Mechanical regulation of gene expression in cardiac myocytes and fibroblasts. *Nat Rev Cardiol*, 16(6):361-378. https://doi.org/10.1038/s41569-019-0155-8

Schlüter KD, Wenzel S, 2008. Angiotensin II: a hormone involved in and contributing to pro-hypertrophic cardiac networks and target of anti-hypertrophic cross-talks. *Pharmacol Ther*, 119(3):311-325. https://doi.org/10.1016/j.pharmthera.2008.05.010

She G, Ren YJ, Wang Y, et al., 2019. K_{Ca}3.1 channels promote cardiac fibrosis through mediating inflammation and differentiation of monocytes into myofibroblasts in angiotensin II-treated rats. *J Am Heart Assoc*, 8(1): e010418. https://doi.org/10.1161/jaha.118.010418

Shi XY, Xiong LX, Xiao L, et al., 2016. Downregulation of caveolin-1 upregulates the expression of growth factors and regulators in co-culture of fibroblasts with cancer cells. *Mol Med Rep*, 13(1):744-752. https://doi.org/10.3892/mmr.2015.4610

Shihata WA, Putra MRA, Chin-Dusting JPF, 2017. Is there a potential therapeutic role for caveolin-1 in fibrosis? *Front Pharmacol*, 8:567. https://doi.org/10.3389/fphar.2017.00567

Shimizu I, Minamino T, 2016. Physiological and pathological cardiac hypertrophy. *J Mol Cell Cardiol*, 97:245-262. https://doi.org/10.1016/j.yjmcc.2016.06.001

Shindo T, Ito K, Ogata T, et al., 2016. Low-intensity pulsed ultrasound enhances angiogenesis and ameliorates left ventricular dysfunction in a mouse model of acute myocardial infarction. *Arterioscler Thromb Vasc Biol*, 36(6):1220-1229. https://doi.org/10.1161/atvbaha.115.306477

Swärd K, Albinsson S, Rippe C, 2014. Arterial dysfunction but maintained systemic blood pressure in cavin-1-deficient mice. *PLoS ONE*, 9(3):e92428. https://doi.org/10.1371/journal.pone.0092428

Sweeney M, Corden B, Cook SA, 2020. Targeting cardiac fibrosis in heart failure with preserved ejection fraction: mirage or miracle? *EMBO Mol Med*, 12(10):e10865. https://doi.org/10.15252/emmm.201910865

Tallquist MD, 2020. Cardiac fibroblast diversity. *Annu Rev Physiol*, 82:63-78. https://doi.org/10.1146/annurev-physiol-021119-034527

Vandergriff AC, Vandergriff MT, Cheng K, 2015. Isolation and cryopreservation of neonatal rat cardiomyocytes. *J Vis Exp*, 9(98):52726. https://doi.org/10.3791/52726

Vogel ER, Manlove LJ, Kuipers I, et al., 2019. Caveolin-1 scaffolding domain peptide prevents hyperoxia-induced airway remodeling in a neonatal mouse model. *Am J Physiol Lung Cell Mol Physiol*, 317(1):L99-L108. https://doi.org/10.1152/ajplung.00111.2018

Volonte D, Galbiati F, 2020. Caveolin-1, a master regulator of cellular senescence. *Cancer Metastasis Rev*, 39(2):397-414. https://doi.org/10.1007/s10555-020-09875-w

Wang JX, Chen HJ, Cao P, et al., 2016. Inflammatory cytokines induce caveolin-1/β-catenin signalling in rat nucleus pulposus cell apoptosis through the p38 MAPK pathway. *Cell Prolif*, 49(3):362-372. https://doi.org/10.1111/cpr.12254

Wang Q, Yu Y, Zhang PP, et al., 2017. The crucial role of activin A/ALK4 pathway in the pathogenesis of Ang-II-induced atrial fibrosis and vulnerability to atrial fibrillation. *Basic Res Cardiol*, 112(4):47. https://doi.org/10.1007/s00395-017-0634-1

Xu TH, Zhao K, Guo XS, et al., 2019. Low-intensity pulsed ultrasound inhibits adipogenic differentiation via HDAC1 signalling in rat visceral preadipocytes. *Adipocyte*, 8(1): 292-303. https://doi.org/10.1080/21623945.2019.1643188

Yan HL, Li YF, Wang C, et al., 2017. Contrary microRNA expression pattern between fetal and adult cardiac remodeling: therapeutic value for heart failure. *Cardiovasc Toxicol*, 17(3):267-276. https://doi.org/10.1007/s12012-016-9381-z

Zaragoza C, Saura M, Ramírez-Carracedo R, 2021. Cardiac microvasculature and adverse remodeling after acute myocardial infarction. New evidence on the use of VEGF as a therapeutic target. *Rev Esp Cardiol (Engl Ed)*, 74(2): 124-125. https://doi.org/10.1016/j.rec.2020.07.019

Zhao K, Yang CX, Li P, et al., 2020. Epigenetic role of N^6-methyladenosine (m^6A) RNA methylation in the cardiovascular system. *J Zhejiang Univ-Sci B (Biomed & Biotechnol)*, 21(7):509-523. https://doi.org/10.1631/jzus.B1900680

Zhao K, Weng LQ, Xu TH, et al., 2021. Low-intensity pulsed ultrasound prevents prolonged hypoxia-induced cardiac fibrosis through HIF-1α/DNMT3a pathway via a TRAAK-dependent manner. *Clin Exp Pharmacol Physiol*, early access. https://doi.org/10.1111/1440-1681.13562

Zhao Y, Liu K, Yin D, et al., 2019. Angiopoietin-like 7 contributes to angiotensin II-induced proliferation, inflammation and apoptosis in vascular smooth muscle cells. *Pharmacology*, 104(5-6):226-234. https://doi.org/10.1159/000501296

Zheng C, Wu SM, Lian H, et al., 2019. Low-intensity pulsed ultrasound attenuates cardiac inflammation of CVB3-induced viral myocarditis via regulation of caveolin-1 and MAPK pathways. *J Cell Mol Med*, 23(3):1963-1975. https://doi.org/10.1111/jcmm.14098

Supplementary information

Figs. S1–S9; Tables S1–S3